nature COMMUNICATIONS

ARTICLE

Received 14 Jul 2015 | Accepted 16 Jun 2016 | Published 20 Jul 2016

DOI: 10.1038/ncomms12246 OPEN

Zero-bias photocurrent in ferromagnetic topological insulator

N. Ogawa[1], R. Yoshimi[2], K. Yasuda[2], A. Tsukazaki[3], M. Kawasaki[1,2] & Y. Tokura[1,2]

Magnetic interactions in topological insulators cause essential modifications in the originally mass-less surface states. They offer a mass gap at the Dirac point and/or largely deform the energy dispersion, providing a new path towards exotic physics and applications to realize dissipation-less electronics. The nonequilibrium electron dynamics at these modified Dirac states unveil additional functions, such as highly efficient photon to spin-current conversion. Here we demonstrate the generation of large zero-bias photocurrent in magnetic topological insulator thin films on mid-infrared photoexcitation, pointing to the controllable band asymmetry in the momentum space. The photocurrent spectra with a maximal response to the intra-Dirac-band excitations can be a sensitive measure for the correlation between Dirac electrons and magnetic moments.

[1] RIKEN Center for Emergent Matter Science (CEMS), Wako, Saitama 351-0198, Japan. [2] Department of Applied Physics and Quantum-Phase Electronics Center (QPEC), University of Tokyo, Tokyo 113-8656, Japan. [3] Institute for Materials Research, Tohoku University, Sendai 980-8577, Japan. Correspondence and requests for materials should be addressed to N.O. (email: naoki.ogawa@riken.jp).

Bismuth-chalcogenides-based topological insulators[1] (TIs) generally have the bulk band gap of several hundreds meV, where the conduction and valence bands are connected by the surface states: mass-less Dirac dispersions with spin-momentum locking. When doped with magnetic elements[2], a Dirac-mass gap opens and/or the energy dispersion deforms (Fig. 1a) through the breaking of time-reversal symmetry[3–5]. The toplogical character of the surface states survives up to a moderate doping density, and offer a fertile ground of quantum phenomena, for example, creation of magnetic monopoles[6], quantized magnetoelectric effects[7–12] and quantum anomalous Hall effects[13–15].

The corresponding Hamiltonian can be expressed as[16]

$$H = \frac{k^2}{2m^*} + v_k(k_x\sigma_y - k_y\sigma_x) + \frac{\lambda}{2}(k_+^3 + k_-^3)\sigma_z - Jn\mathbf{S}\cdot\sigma, \quad (1)$$

where each term represents particle-hole asymmetry (k is momentum, and m^* the effective mass), spin-orbit interaction resulting in the helical spin state (v_k is velocity and σ the Pauli matrices), hexagonal warping with amplitude λ ($k_\pm \equiv k_x \pm ik_y$), and coupling of electron's spin to localized dopant spin $\mathbf{S}$ (n is the density and J is the interaction energy), respectively[5,16,17], with the unit of $\hbar = 1$. Here we take Cartesian coordinates with z along the surface normal. For the out-of-plane alignment of the dopant moments, either by magnetic anisotropy or by external fields, the spins turn parallel to z near the gapped Dirac point in the energy spectrum, and the Dirac-mass gap scales with JnS_z. This dispersion shows 3-fold symmetry around the k_z axis[5], leading to an isotropic optical response in the linear regime. The Dirac-mass gap 2Δ of 60 meV was experimentally confirmed recently on a local scale in the case of Cr-doped $(Bi,Sb)_2Te_3$ ferromagnetic TIs[18]. For the case of in-plane magnetization, for example, the finite S_y, the gap closes or substantially reduces, with the Dirac point shifted from the zone center along k_x due to the Zeeman effect (Fig. 1a). Accordingly, the constant energy contour deforms by leaving one mirror plane in the momentum space[5]. This asymmetry can induce transient spin and charge currents on photoexcitation[19].

In addition to intensive optical spectroscopy[20–27], a number of photoeffects in TIs have been studied both theoretically and experimentally; photocurrent generation and galvanic effects[28–32], carrier/spin dynamics elaborated by time-resolved optics[33–41], photoemission[42–51] and the Floquet state[52], including the cases of thin films with magnetic dopants[53,54], to name a few. For the photocurrent generation at the normal incidence, it is predicted that the orbital coupling of light, that is, $\hbar\mathbf{k} \rightarrow \hbar\mathbf{k} - e\mathbf{A}$, provides a predominant contribution to the polarization-independent photocurrent under an in-plane external magnetic field[17].

In this paper, we study photocurrent spectra in $Cr_{0.3}(Bi_{0.22}Sb_{0.78})_{1.7}Te_3$ (CBST) thin films with a thickness of 8 nm. These samples are designed to achieve the following properties: The Fermi level is tuned near the Dirac point, which is isolated from the bulk states[18,55]. The top and bottom surfaces hosting Dirac states are decoupled with the minimal contribution of the bulk volume in between. The dopant concentration is increased from those of the previous works[13–15] to enhance magnetic transition temperature, T_C. Thus, intrinsic signals from the Dirac electrons[49] interacting with magnetic dopants can be explored at moderate temperature. We show the generation of large zero-bias photocurrent on mid-infrared photoexcitation at normal incidence (Fig. 1b), realized by the field-controllable band asymmetry in the momentum space. The enhanced response at the intra-Dirac-band excitation would reveal intrinsic interactions between Dirac electrons and magnetic moments.

Results

Transport properties. Figure 1c shows that the fabricated CBST film is non-metallic at room temperature, and the conduction

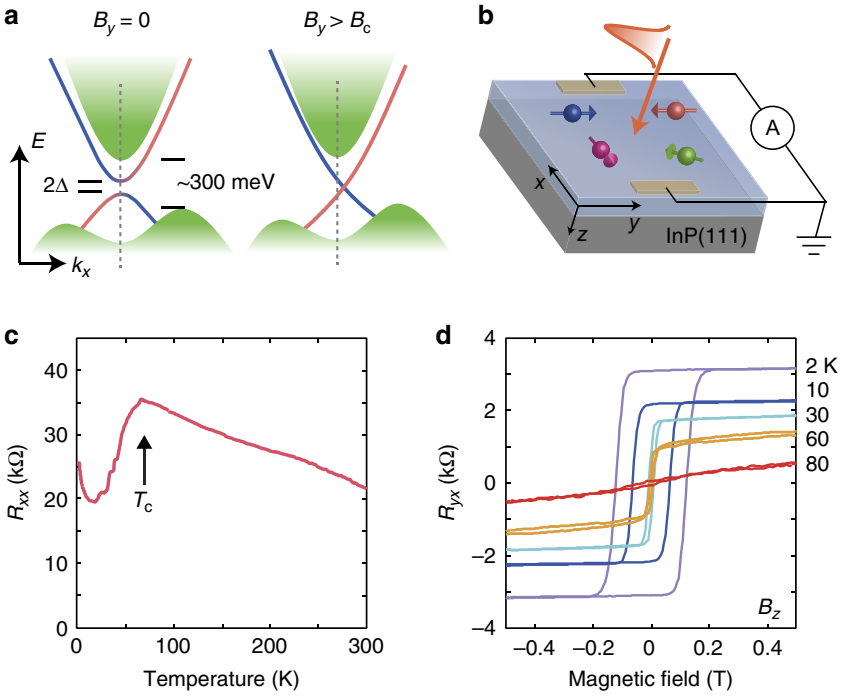

Figure 1 | Schematic energy dispersion and transport properties. (**a**) Electronic structure of magnetic topological insulator: the mass gap 2Δ at the Dirac point, and the effects of in-plane magnetic field above the critical value B_c inducing finite in-plane portion of the dopant spin S_y. (**b**) Experimental setup with the coordinates used in this work. The film is illuminated at normal incidence, and the photocurrent along x direction is measured. (**c**) Longitudinal and (**d**) Hall resistance of the $Cr_{0.3}(Bi_{0.22}Sb_{0.78})_{1.7}Te_3$/InP(111) film, indicating the magnetic transition temperature T_C and ferromagnetic response of the surface Dirac states with uniaxial anisotropy.

through the surface states becomes apparent slightly below the $T_C \sim 75$ K, due to the freezing of thermally excited carriers in the bulk state and also reduced magnetic impurity scatterings[14] (Supplementary Fig. 1). The Hall resistivity data (Fig. 1d) also illustrate the T_C and clear magnetic hysteresis loops at lower temperatures. In fact, the thin-film sample, prepared at the similar growth condition but with smaller Cr concentration, was proven to show the quantum anomalous Hall effect as the hallmark of the above features of our sample design[14].

Zero-bias photocurrent spectra. Figure 2a,b show the representative zero-bias photocurrent under the in-plane (B_y) and out-of-plane (B_z) external magnetic fields measured at 20 K, compared with the sample magnetization (ΔM, after subtracting the substrate contributions). Only in the case of applying B_y, a large photocurrent was detected. The current is nearly proportional to the in-plane magnetization; it reverses when the magnetic-field direction (or spin S_y) is flipped. A slight asymmetry at the positive and negative fields could be ascribed to the nonequivalent electrodes geometry. The photocurrent spectra show a pronounced peak around 250 meV (Fig. 2c). These characteristics were found to be independent of the incident photon polarization[17]. The bulk band gap is anticipated to be around 300 meV, therefore the low-energy photoresponses, at least <300 meV, can be ascribed to the dynamics of the spin-polarized Dirac electron at the surface. There exist some fluctuations in the photocurrent spectra, such as the increase of photocurrent around 100 meV under 0 T, whose origins are not clear at this stage.

Temperature and magnetic-field dependence. Detailed characteristics of the zero-bias photocurrent are shown in Fig. 3. The inflection behaviour in the magnetic-field dependence diminishes around 80 K (Fig. 3a), consistent with the trend of in-plane magnetization (Fig. 3b) and the Hall resistance data (Fig. 1d). The temperature dependence of the photocurrent nicely follows that of the magnetization (Fig. 3c).

Discussion

For the case of normal incidence in general, an imbalance in the electron excitation at the opposite k, and nonequilibrium carrier distributions on relaxation, can trigger the generation of directional photocurrent[19]. This photocurrent can be enhanced by the spin-orbit interaction, most prototypically for the surface Dirac electrons with the deformed Dirac dispersions as in the present case. In our experiments, possible contributions from the photogalvanic effect due to the trigonal warping can be neglected, judging from the absence of photocurrent at zero field. Neither the Nernst-Ettingshausen effect nor the photon drags have roles in our optical geometry.

The observed zero-bias photocurrent in the magnetic TI thin film can be explained by the magnetization-induced modification of the energy dispersion (Fig. 4), making both the excitation and relaxation at $\pm k$ asymmetric. In the absence of external fields, or under the application of B_z, the doped Cr moment induces the Dirac-mass gap. In this case, the constant energy contour of the dispersion remains symmetric in the k_x-k_y plane (Fig. 4a,d). In stark contrast, with the application of $-B_y$ (induction of S_y), the Dirac-mass gap closes, and the energy contour shifts/deforms

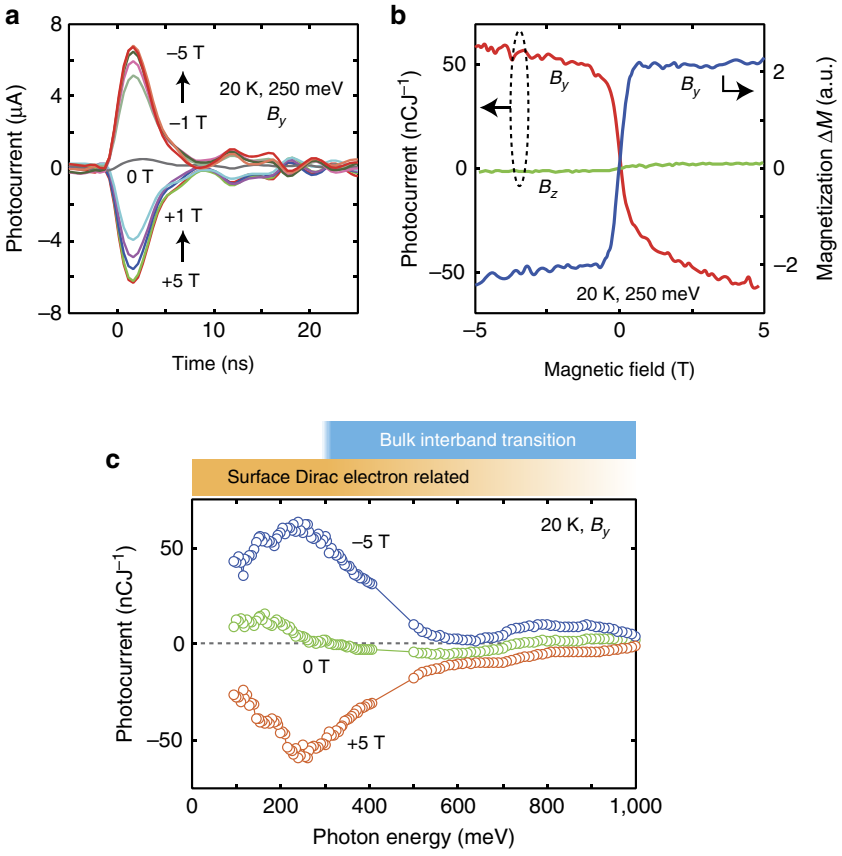

Figure 2 | Photocurrent characteristics of the magnetic topological insulator thin film. (**a**) Zero-bias photocurrent at 250 meV (and 350 nJ) excitation under varying in-plane magnetic field B_y. (**b**) Normalized photocurrent under in-plane (B_y) and out-of-plane (B_z) magnetic fields, plotted together with the magnetization under B_y. (**c**) Photocurrent spectra at 20 K under B_y.

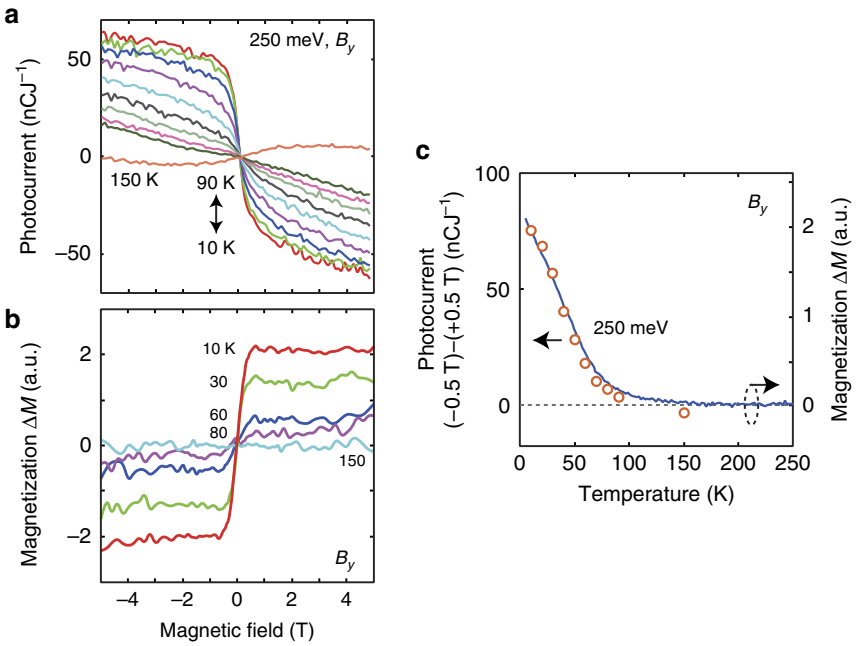

Figure 3 | Temperature dependence of the zero-bias photocurrent. (**a**) Normalized zero-bias photocurrent under in-plane magnetic field B_y at varying temperature. (**b**) Magnetization under B_y. (**c**) Photocurrent at ± 0.5 T as a function of temperature, plotted together with magnetization.

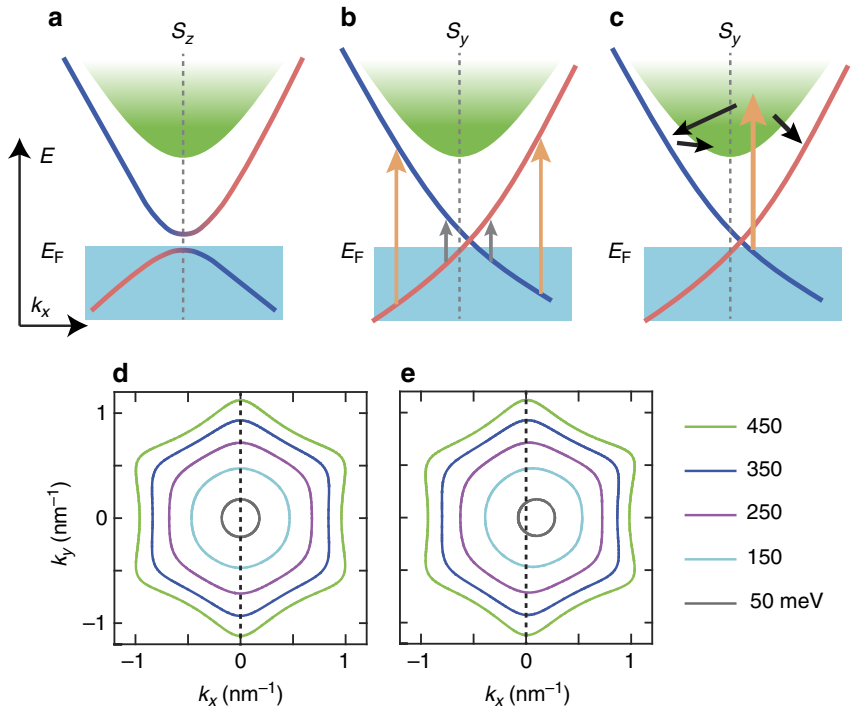

Figure 4 | Mechanism of zero-bias photocurrent generation. Schematics for the energy dispersion in the magnetic topological insulator for the out-of-plane S_z (**a**) and in-plane S_y (**b**,**c**) alignment of dopant spin. Corresponding energy contours calculated from equation (1) are depicted in (**d**,**e**). Possible imbalance in the photoexcitation at the opposite k_x is shown in **b**: grey and orange arrows for low- and high-photon-energy excitations, respectively. The scattering between the surface and bulk states is shown in **c**.

orthogonal to the orientation of magnetic moment (towards k_x for S_y) (Fig. 4b,e). Here we draw the energy contours in Fig. 4d,e, by following equation (1) with the parameters in refs 5,19, and $2\Delta = 60$ meV from ref. 18. These shifts and deformations are proportional to the in-plane moment S_y, and the latter have a major role for the photocurrent generation.

When the photon energy is below 300 meV, within the bulk band gap where the observed photocurrent largely enhances, the photoexcitation between the bulk valence and conduction bands can be neglected. Given that the Fermi level is located near the Dirac point, we can expect two pathways of Dirac electron-related excitation and relaxation; excitation within the surface states

(Fig. 4b), and between the surface states and the bulk states (and vice versa) (Fig. 4c). We will exclude the latter process as the major mechanism of photocurrent generation in the following, since merely small photocurrent observed at the higher photon energy (Fig. 2c). The surface state as the final state of the optical excitation is important for the observed photocurrent, where the asymmetry in the dispersion is directly involved.

Now we discuss the spectral structure as exemplified by the peak around 250 meV (Fig. 2c). The optical processes possibly involved in the present photogalvanic effect have been discussed theoretically in refs 5,19. In short, the zero-bias photocurrent flows due to the unbalanced transient carrier population ($f(k)$: Fermi-Dirac function) in the deformed Dirac dispersions, that is, $f(k_x) - f(-k_x)$, multiplied by the group velocity, which can be proportional to the local magnetic moment. The optical absorption in the surface Dirac states is supposed to be nearly monotonic as a function of photon energy in our spectral range[19,21–25,54] (see also Supplementary Fig. 2). However, the observed photocurrent shows a clear peak around 250 meV; it decreases towards zero in lowering photon energy and also shows a reduction in increasing photon energy above 250 meV. The former trend is predicted in ref. 19 as due to the decreased asymmetry near the Dirac point (compare the grey and orange transitions in Fig. 4b). Even with the finite optical absorption, the photocarriers with the opposite group velocity would cancel for the low-energy excitation. The decrease in the photocurrent at higher energy can be ascribed to the pronounced scattering between bulk and surface states (Fig. 4c), which is not taken into account in ref. 19. Here the optical transition to the bulk states increases in the photon energy region above $\sim$250 meV, and most of the population asymmetry is lost above 500 meV due to the scattering between the bulk and surface states. Note that we have finite potential fluctuations in the film, including those of $\sim$20 meV from Cr dopants[18] and also between the two surface states (see below), which can induce broadenings in the photocurrent spectra. The small but finite photocurrent under B_z (Fig. 2b) may point to the effect of hexagonal warping with the spin moments oriented along z, which is ignored in the above analyses[5].

Considering the thickness of our sample (8 nm), the top and the bottom surface states (the latter is the interface between CBST and InP) experience nearly the same optical fields for the low-photon-energy region (Supplementary Fig. 2). In the above-discussed model, the energy contour shifts/deforms in the opposite direction for the top and bottom surface states; the excited photocarriers flow in the counter direction, which may cancel at the end. However, in general, the top and bottom surface states are inevitably inequivalent[9] due to their distinct environments and growth characteristics. The energy shift of the surface-state electronic bands is estimated as large as 50-70 meV from the quantum Hall effect measurements[56]. Thus we detect the photocurrent portion not cancelled in the two surface states. By checking the signals from the sample with a modulated Cr doping, we found an indication that the bottom surface has the larger contribution to the photocurrent in the present case (Supplementary Fig. 3). It is also seen that we can possibly enhance the photocurrent by further differentiating the top and bottom surface states. However, a quantitative discussion is difficult at this stage because of the extrinsic factors such as the change in the transition temperature and scatterings by dopants.

The amplitude of the detected photocurrent, although transient, reaches a value as large as 60 μA cm^{-1} (Fig. 2a with the experimental geometry taken into account). This is more than two orders of magnitude larger than that observed by the circular photogalvanic effect in the bulk Bi_2Se_3 (ref. 30), in which the oblique-incidence circularly polarized light can inject the spins in the Dirac dispersion to generate the zero-bias current. This is also larger than the theoretically predicted values with magnetic proximity interactions[19] (see also Supplementary Fig. 4). Considering the relaxation of photoexcited carriers before reaching the electrodes, the instantaneous photocurrent would be even much larger. In the experiments shown above, we used the external magnetic field larger than $\sim$0.5 T to orient the Cr moments (and to generate the photocurrent). If we could prepare the sample with an easy-plane anisotropy, it would be possible to have a spin-polarized photocurrent in zero field, whose direction could be controlled by the switching of the magnetic domains. As such, the magnetic control of the nonequilibrium Dirac electrons in the magnetic topological insulator will pave a new path for intriguing spintronic functions.

Methods

Sample preparation and characterization. Thin films of CBST were grown on InP(111) substrates by the molecular beam epitaxy, where the similar films with the smaller Cr concentration have been proven to show the quantum anomalous Hall effect. The detailed growth conditions are described in ref. 14. The surface was protected by a 3 nm thick Al_2O_3 cap layer. The samples were characterized by conventional transport and magnetization measurements. The diamagnetic contribution of the substrate was subtracted for the latter.

Photocurrent detection. Two AuPd electrodes were deposited along the [10$\bar{1}$0] axis after removing the cap layer. The short-circuit photocurrent was measured through a wide-band preamplifier (bandwidth of 200 MHz) with the illumination by a pulsed laser source (120 fs, 1 kHz, spot size 1.0–0.5 mm in diameter) at normal incidence. The excitation spot was carefully positioned at the center of the sample to cancel possible thermoelectric signals (Supplementary Fig. 5). The time trace of the photocurrent was averaged 150 times in the digitizing oscilloscope, which was broadened by the response of the preamplifier and followed by ringing due to the impedance mismatch in the circuit (Fig. 2a). The magnetic field and photon energy dependencies were obtained by averaging more than 2,048 signal pulses after gating the photocurrent signal by a boxcar averager. The acquired signal was normalized by the integrated time-trace from the oscilloscope, as a number of charge, and also by the incident photon intensity. The error bars in our measurements are within the circle marks in Fig. 2c. We have checked three samples with slightly different compositions, and confirmed nearly the identical results.

Data availability. The data that support the findings of this study are available from the corresponding author on request.

References

1. Hasan, M. Z. & Kane, C. L. Topological insulators. *Rev. Mod. Phys.* **82,** 3045–3067 (2010).
2. Li, M. *et al.* Experimental verification of the Van Vleck nature of long-range ferromagnetic order in the vanadium-doped three-dimensional topological insulator Sb_2Te_3. *Phys. Rev. Lett.* **114,** 146802 (2015).
3. Hor, Y. S. *et al.* Development of ferromagnetism in the doped topological insulator $Bi_{2-x}Mn_xTe_3$. *Phys. Rev. B* **81,** 195203 (2010).
4. Chen, Y. L. *et al.* Massive Dirac fermion on the surface of a magnetically doped topological insulator. *Science* **329,** 659–662 (2010).
5. Henk, J. *et al.* Topological character and magnetism of the Dirac state in Mn-Doped Bi_2Te_3. *Phys. Rev. Lett.* **109,** 076801 (2012).
6. Qi, X.-L., Li, R., Zhang, J. & Zhang, S.-C. Inducing a magnetic monopole with topological surface states. *Science* **323,** 1184–1187 (2009).
7. Qi, X.-L., Hughes, T. L. & Zhang, S.-C. Topological field theory of time-reversal invariant insulators. *Phys. Rev. B* **78,** 195424 (2008).
8. Tse, W.-K. & MacDonald, A. H. Giant magneto-optical Kerr effect and universal Faraday effect in thin-film topological insulators. *Phys. Rev. Lett.* **105,** 057401 (2010).
9. Maciejko, J., Qi, X.-L., Drew, H. D. & Zhang, S.-C. Topological quantization in units of the fine structure constant. *Phys. Rev. Lett.* **105,** 166803 (2010).
10. Li, R., Wang, J., Qi, X.-L. & Zhang, S.-C. Dynamical axion field in topological magnetic insulators. *Nat. Phys* **6,** 284–288 (2010).
11. Valdés Aguilar, R. *et al.* Terahertz response and colossal Kerr rotation from the surface states of the topological insulator Bi_2Se_3. *Phys. Rev. Lett.* **108,** 087403 (2012).
12. Orlita, M. *et al.* Magneto-optics of massive Dirac fermions in bulk Bi_2Se_3. *Phys. Rev. Lett.* **114,** 186401 (2015).
13. Chang, C.-Z. *et al.* Experimental observation of the quantum anomalous Hall effect in a magnetic topological insulator. *Science* **340,** 167–170 (2013).

14. Chekelsky, J. G. *et al.* Trajectory of the anomalous Hall effect towards the quantized state in a ferromagnetic topological insulator. *Nat. Phys* **10,** 731–736 (2014).
15. Chang, C.-Z. *et al.* High-precision realization of robust quantum anomalous Hall state in a hard ferromagnetic topological insulator. *Nat. Mater.* **14,** 473–477 (2015).
16. Fu, L. Hexagonal warping effects in the surface states of the topological insulator Bi_2Te_3. *Phys. Rev. Lett.* **103,** 266801 (2009).
17. Junck, A., Refael, G. & von Oppen, F. Photocurrent response of topological insulator surface states. *Phys. Rev. B* **88,** 075144 (2013).
18. Lee, I. *et al.* Imaging Dirac-mass disorder from magnetic dopant atoms in the ferromagnetic topological insulator $Cr_x(Bi_{0.1}Sb_{0.9})_{2-x}Te_3$. *Proc. Natl Acad. Sci.* **112,** 1316–1321 (2015).
19. Semenov, Y. G., Li, X. & Kim, K. W. Tunable photogalvanic effect on topological insulator surfaces via proximity interactions. *Phys. Rev. B* **86,** 201401 (R) (2012).
20. Chang, M.-C. & Yang, M.-F. Optical signature of topological insulators. *Phys. Rev. B* **80,** 113304 (2009).
21. LaForge, A. D. *et al.* Optical characterization of Bi_2Te_3 in a magnetic field: infrared evidence for magnetoelectric coupling in a topological insulator material. *Phys. Rev. B* **81,** 125120 (2010).
22. Di Pietro, P. *et al.* Optical conductivity of bismuth-based topological insulators. *Phys. Rev. B* **86,** 045439 (2012).
23. Akrap, A. *et al.* Optical properties of Bi_2Te_2Se at ambient and high pressures. *Phys. Rev. B* **86,** 235207 (2012).
24. Li, Z. & Carbotte, J. P. Hexagonal warping on optical conductivity of surface states in topological insulator Bi_2Te_3. *Phys. Rev. B* **87,** 155416 (2013).
25. Post, K. W. *et al.* Infrared probe of the bulk insulating response in $Bi_{2-x}Sb_xTe_{3-y}Se_y$ topological insulator alloys. *Phys. Rev. B* **91,** 165202 (2015).
26. Onishi, Y. *et al.* Ultrafast carrier relaxation through Auger recombination in the topological insulator $Bi_{1.5}Sb_{0.5}Te_{1.7}Se_{1.3}$. *Phys. Rev. B* **91,** 085306 (2015).
27. Wu, L. *et al.* High-resolution Faraday rotation and electron-phonon coupling in surface states of the bulk-insulating topological insulator $Cu_{0.02}Bi_2Se_3$. *Phys. Rev. Lett.* **115,** 217602 (2015).
28. Kastl, C. *et al.* Local photocurrent generation in thin films of the topological insulator Bi_2Se_3. *Appl. Phys. Lett.* **101,** 251110 (2012).
29. Bas, D. A. *et al.* Coherent control of injection currents in high-quality films of Bi_2Se_3. *Appl. Phys. Lett.* **106,** 041109 (2015).
30. McIver, J. W., Hsieh, D., Steinberg, H., Jarillo-Herrero, P. & Gedik, N. Control over topological insulator photocurrents with light polarization. *Nat. Nanotech.* **7,** 96–100 (2012).
31. Kastl, C., Karnetzky, C., Karl, H. & Holleitner, A. W. Ultrafast helicity control of surface currents in topological insulators with near-unity fidelity. *Nat. Commun.* **6,** 6617 (2015).
32. Okada, K. N. *et al.* Enhanced photogalvanic current in topological insulators via Fermi energy tuning. *Phys. Rev. B* **93,** 081403 (R) (2016).
33. Qi, J. *et al.* Ultrafast carrier and phonon dynamics in Bi_2Se_3 crystals. *Appl. Phys. Lett.* **97,** 182102 (2010).
34. Hsieh, D. *et al.* Nonlinear optical probe of tunable surface electrons on a topological insulator. *Phys. Rev. Lett.* **106,** 057401 (2011).
35. Kumar, N. *et al.* Spatially resolved femtosecond pump-probe study of topological insulator Bi_2Se_3. *Phys. Rev. B* **83,** 235306 (2011).
36. Hsieh, D. *et al.* Selective probing of photoinduced charge and spin dynamics in the bulk and surface of a topological insulator. *Phys. Rev. Lett.* **107,** 077401 (2011).
37. Sim, S. *et al.* Ultrafast terahertz dynamics of hot Dirac-electron surface scattering in the topological insulator Bi_2Se_3. *Phys. Rev. B* **89,** 165137 (2014).
38. Glinka, Y. D., Babakiray, S., Johnson, T. A., Holcomb, M. B. & Lederman, D. Effect of carrier recombination on ultrafast carrier dynamics in thin films of the topological insulator Bi_2Se_3. *Appl. Phys. Lett.* **105,** 171905 (2014).
39. Boschini, F. *et al.* Coherent ultrafast spin-dynamics probed in three dimensional topological insulators. *Sci. Rep.* **5,** 15304 (2015).
40. Maezawa, S. *et al.* Optically detecting the edge-state of a three-dimensional topological insulator under ambient conditions by ultrafast infrared photoluminescence spectroscopy. *Sci. Rep.* **5,** 16443 (2015).
41. Wang, M. C., Qiao, S., Jiang, Z., Juo, S. N. & Qi, J. Unraveling photoinduced spin dynamics in the topological insulator Bi_2Sb_3. *Phys. Rev. Lett.* **116,** 036601 (2016).
42. Sobota, J. A. *et al.* Ultrafast optical excitation of a persistent surface-state population in the topological insulator Bi_2Se_3. *Phys. Rev. Lett.* **108,** 117403 (2012).
43. Sobota, J. A. *et al.* Direct optical coupling to an unoccupied Dirac surface state in the topological insulator Bi_2Se_3. *Phys. Rev. Lett.* **111,** 136802 (2013).
44. Cacho, C. *et al.* Momentum-resolved spin-dynamics of bulk and surface excited states in the topological insulator Bi_2Se_3. *Phys. Rev. Lett.* **114,** 097401 (2014).
45. Hajlaoui, M. *et al.* Tuning a Schottky barrier in a photoexcited topological insulator with transient Dirac cone electron-hole asymmetry. *Nat. Commun.* **5,** 3003 (2014).
46. Reimann, J., Güdde, J., Kuroda, K., Chulkov, E. V. & Höfer, U. Spectroscopy and dynamics of unoccupied states of the topological insulators Sb_2Te_3 and Sb_2Te_2S. *Phys. Rev. B* **90,** 081106 (R) (2014).
47. Shoman, T. *et al.* Topological proximity effect in a topological insulator hybrid. *Nat. Commun.* **6,** 6547 (2015).
48. Xu, C.-Z. *et al.* Photoemission circular dichroism and spin polarization of the topological surface states in ultrathin Bi_2Te_3 films. *Phys. Rev. Lett.* **115,** 016801 (2015).
49. Neupane, M. *et al.* Gigantic surface lifetime of an intrinsic topological insulator. *Phys. Rev. Lett.* **115,** 116801 (2015).
50. Kogar, A. *et al.* Surface collective modes in the topological insulators Bi_2Se_3 and $Bi_{0.5}Sb_{1.5}Te_{3-x}Se_x$. *Phys. Rev. Lett.* **115,** 257402 (2015).
51. Kuroda, K., Reimann, J., Gudde, J. & Hofer, U. Generation of transient photocurrents in the topological surface state of Sb_2Te_3 by direct optical excitation with midinfrared pulses. *Phys. Rev. Lett.* **116,** 076801 (2016).
52. Wang, Y. H., Steinberg, H., Jarillo-Herrero, P. & Gedik, N. Observation of Floquet-Bloch states on the surface of a topological insulator. *Science* **342,** 453–457 (2013).
53. Zhang, D. *et al.* Interplay between ferromagnetism, surface states, and quantum corrections in a magnetically doped topological insulator. *Phys. Rev. B* **86,** 205127 (2012).
54. Lasia, M. & Brey, L. Optical properties of magnetically doped ultrathin topological insulator slabs. *Phys. Rev. B* **90,** 075417 (2014).
55. Yoshimi, R. *et al.* Dirac electron states formed at the heterointerface between a topological insulator and a conventional semiconductor. *Nat. Mater.* **13,** 253–257 (2014).
56. Yoshimi, R. *et al.* Quantumj Hall effect on top and bottom surface states of topological insulator $(Bi_{1-x}Sb_x)_2Te_3$ films. *Nat. Commun.* **6,** 6627 (2015).

Acknowledgements

We thank N. Nagaosa and W. Koshibae for stimulating discussions. This research is supported by JSPS KAKENHI Grant Numbers 24224009 and 16K13705.

Author contributions

N.O., R.Y., A.T., M.K. and Y.T. conceived the experiment; R.Y., K.Y. prepared and characterized the samples; and N.O. carried out the optical experiments. N.O., R.Y., K.Y., A.T., M.K. and Y.T. wrote the manuscript. All authors contributed considerably.

Additional information

Supplementary Information accompanies this paper at http://www.nature.com/naturecommunications

Competing financial interests: The authors declare no competing financial interests.

Reprints and permission information is available online at http://npg.nature.com/reprintsandpermissions/

How to cite this article: Ogawa, N. *et al.* Zero-bias photocurrent in ferromagnetic topological insulator. *Nat. Commun.* 7:12246 doi: 10.1038/ncomms12246 (2016).